JACS
JOURNAL OF THE AMERICAN CHEMICAL SOCIETY
pubs.acs.org/JACS
Article

# Over 500 Wh kg$^{-1}$ Solid-State Lithium Metal Batteries with Long Cycling Stability Using *In Situ* Polymerized Electrolyte

Nuo Xu, Xingchen Song, Guolin Sun, Jinping Zhang, Zuhao Quan, Genglin Lou, Aihong Li, Chenxi Li, Hongtao Zhang,* and Yongsheng Chen*

Cite This: *J. Am. Chem. Soc.* 2026, 148, 2471−2480



**ABSTRACT:** Lithium metal batteries (LMBs) are regarded as the "holy grail" of next-generation energy storage systems due to their potential for high energy density. However, uncontrolled lithium dendrite growth on lithium metal anodes leads to poor cycling stability and serious safety risks, hindering their practical deployment. Herein, we design an *in situ* polymerized POSS-based gel polymer electrolyte (POSS-GPE) that exhibits high ionic conductivity (3.04 mS cm$^{-1}$ at room temperature), excellent oxidative stability (>4.9 V vs Li$^+$/Li), broad compatibility with diverse electrode materials, and intrinsic flame retardancy. The POSS-GPE establishes an anion-rich solvation environment that promotes the formation of robust, anion-derived electrode−electrolyte interphase on both the cathode and anode, thus mitigating interfacial degradation. As a result, $LiNi_{0.8}Co_{0.1}Mn_{0.1}O_2$|POSS-GPE|Li (50 $\mu$m) full cell delivers long-term cycling stability of 500 cycles with 87.3% capacity retention. Furthermore, a 6.08 Ah pouch cell with lean electrolyte (1.40 g Ah$^{-1}$) achieves a remarkable energy density of 511.2 Wh kg$^{-1}$ and cycles stably for 70 cycles at 4.6 V, representing the best balance between cycling performance and energy density for polymer-electrolyte-based LMBs. The high-energy-density pouch cells also demonstrate superior safety in nail-penetration tests. This work presents a promising strategy for developing practical high-energy-density and high-safety LMBs.

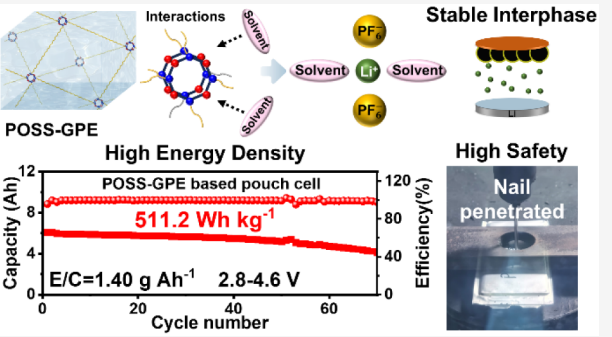


## INTRODUCTION

Lithium metal batteries (LMBs) have garnered significant attention for next-generation energy storage, primarily owing to the high theoretical specific capacity (3860 mAh g$^{-1}$), the lowest redox potential (−3.04 V vs the standard hydrogen electrode), and a low density (0.534 g cm$^{-3}$) of the lithium metal anode (LMA).[1,2] When coupled with high-voltage cathodes, LMBs hold the potential to deliver energy densities of over 500 Wh kg$^{-1}$.[3−6] However, the realization of the application is severely hampered by poor cycle life and safety concerns under practical conditions.[7−9]

Replacing liquid electrolytes with solid-state electrolytes (SSEs) is a prominent strategy to overcome these issues.[10] SSEs are commonly classified into inorganic solid electrolytes (ISE) and solid polymer electrolytes (SPEs).[11] Compared to the rigid inorganic counterparts, SPEs are particularly attractive for their lower costs, simplified manufacturing, and superior electrode−electrolyte interfacial contact.[12] The *in situ* polymerization further enhances their appeal for large-scale application due to the higher ionic conductivity, improved interfacial contact, and compatibility with current battery fabrication process.[13,14] However, polymer electrolytes still suffer from insufficient interfacial stability, leading to short cycle life, especially under practical conditions, such as high capacity, low negative-to-positive capacity ratio (N/P), and low electrolyte-to-capacity ratio (E/C).[15,16]

Modulating the solvation structure of Li$^+$ can promote the formation of an inorganic-rich cathode electrolyte interphase (CEI) and solid electrolyte interphase (SEI), thereby improving the performance and safety of high-voltage LMBs.[17−19] In polymer electrolytes, this modulation can be achieved by engineering the polymer matrix. Motivated by these insights, we focused on siloxanes, a class of widely available and low-cost materials, as building units for the polymer matrix due to their high stability, intrinsic flame retardancy, wide electrochemical window, and weak intermolecular interactions with Li$^+$.[20−23] Among siloxanes, cage-like polyhedral oligomeric silsesquioxane (POSS) is particularly attractive owing to its rigid structure and facile chemical modification.[24−26] Furthermore, the weak interaction with Li$^+$ renders POSS an ideal building block for the polymer matrix to

Received: October 1, 2025
Revised: December 29, 2025
Accepted: December 31, 2025
Published: January 7, 2026

Scheme 1. The Solvation Structure Modulating Mechanism of POSS-GPE in High-Voltage LMBs Compared with $SiO_2$-GPE

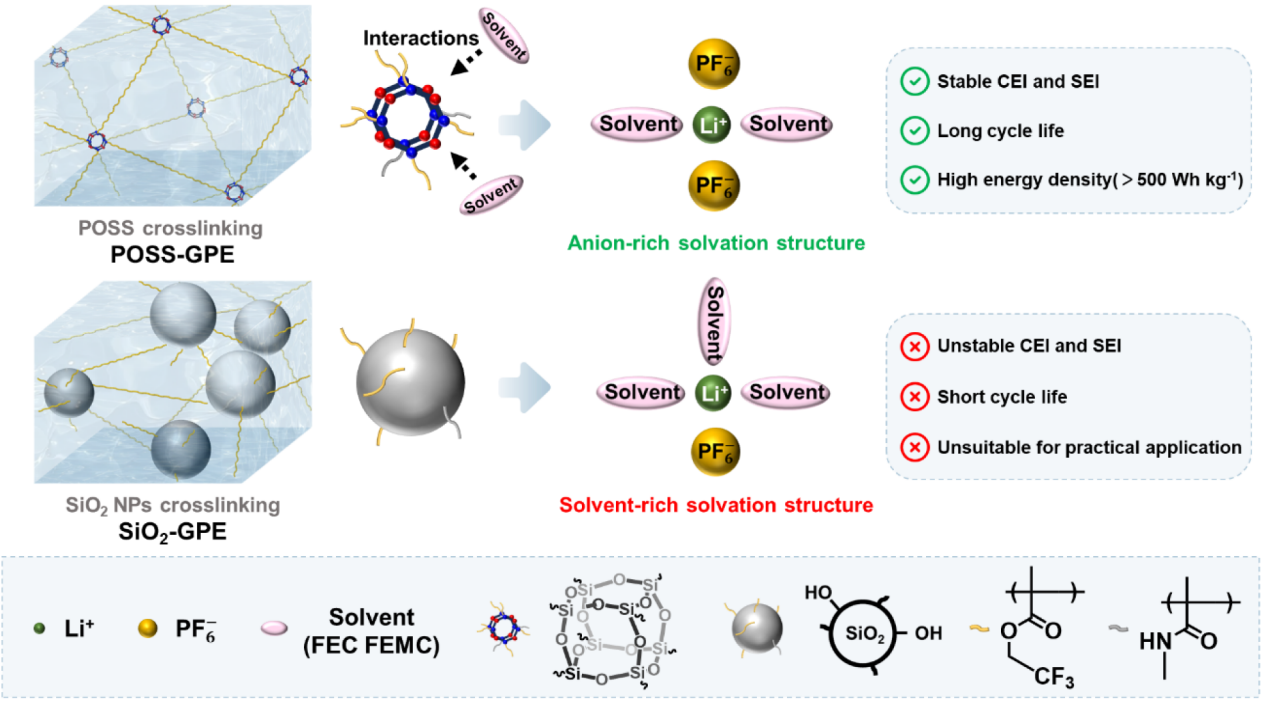


modulate an anion-rich solvation structure,[27] which facilitates robust CEI and SEI formation, enabling practical high-voltage LMBs with both high cycling stability and safety simultaneously.

Thus, in this work, we design an *in situ* polymerized POSS-cross-linked gel polymer electrolyte (POSS-GPE) for high-energy-density LMBs with enhanced safety and cycling stability. The POSS-GPE employs strong POSS−solvent interaction and weak POSS−$Li^+$ coordination to restructure the $Li^+$ solvation sheath into an anion-rich solvation structure, thereby facilitating robust, inorganic-rich CEI and SEI. These interphases suppress parasitic reactions at electrode−electrolyte interface and promote rapid, uniform $Li^+$ deposition on LMAs, yielding a submicron-spherical Li deposition morphology. As a result, POSS-GPE exhibits a high ionic conductivity of 3.04 mS $cm^{-1}$ at room temperature, excellent compatibility with both high-voltage cathodes and LMAs, and nonflammability. Furthermore, the $LiNi_{0.8}Co_{0.1}Mn_{0.1}O_2$(NCM811)|POSS-GPE|Li full cell demonstrates a long cycle life of 500 cycles, retaining 87.3% of its capacity. Moreover, a 6.08 Ah NCM811|POSS-GPE|Li pouch cell with lean electrolyte (E/C = 1.40 g $Ah^{-1}$) delivers a remarkable energy density of 511.2 Wh $kg^{-1}$ with stable cycling of 70 cycles at 4.6 V. This high-energy-density pouch cell also demonstrates superior safety by passing the industry-standard nail-penetration tests. These results highlight the significant potential of POSS-GPE for practical, high-performance LMBs.

## RESULTS AND DISCUSSION

### Polymer Structure Design and Characterization

As shown in Scheme 1, the POSS-GPE is fabricated by using an acryloyloxypropyl-functionalized POSS unit as the cross-linker. In the design of the polymer matrix, 2,2,2-trifluoroethyl methacrylate (TFEMA) is selected as the primary monomer to ensure high oxidation stability. Additionally, *N*-methylmethacrylamide (NMMAm) is incorporated to establish a hydrogen-bond network, which enhances the mechanical robustness of the polymer electrolyte and its ability to accommodate volume changes of the electrodes during cycling.[5] For comparison, methacryloyloxy-functionalized $SiO_2$ nanoparticles ($SiO_2$ NPs) are selected as the cross-linker to prepare the control $SiO_2$-GPE. The polymerization reactions and the resulting polymer structures of both electrolytes are shown in Figure S1. The *in situ* polymerization process is detailed in the Supporting Information.

The successful gelation of the electrolytes is visually confirmed (Figure S2), and the polymerization is verified by Fourier-transform infrared (FT-IR) spectra, which show the disappearance of the C═ C stretching vibration peaks (Figure S3).[28−30] According to $^1$H nuclear magnetic resonance (NMR) analysis, the POSS-GPE shows monomer conversion ratios of ∼88% for TFEMA and ∼86% for NMMAm, while the POSS cross-linker is fully converted (Figure S4). Additionally, the POSS-GPE exhibits robust mechanical properties, featuring a Young's modulus of 529.3 MPa and a tensile strength of 14.2 MPa, as determined by tensile testing in Figure S5.[31] Furthermore, ignition tests confirm the nonflammability of the POSS-GPE, highlighting its intrinsic safety advantages (Figure S6).

To validate our design principle, density functional theory (DFT) calculations are performed (Figure S7) to investigate the intermolecular interactions within the GPEs. The calculated binding energy between $Li^+$ and the POSS unit (−3.14 eV) is significantly weaker than that with $SiO_2$ NP (−4.01 eV). In contrast, the POSS unit exhibits a much stronger interaction with the FEC solvent (−7.16 eV) compared to that of the $SiO_2$ NP (−5.77 eV). These findings confirm the solvent-attracting and $Li^+$-repelling nature of the POSS units.[32] This unique affinity can effectively extract solvent molecules from the primary solvation sheath of $Li^+$ with minimized participation in the solvation structure. These


https://doi.org/10.1021/jacs.5c17294
J. Am. Chem. Soc. 2026, 148, 2471−2480

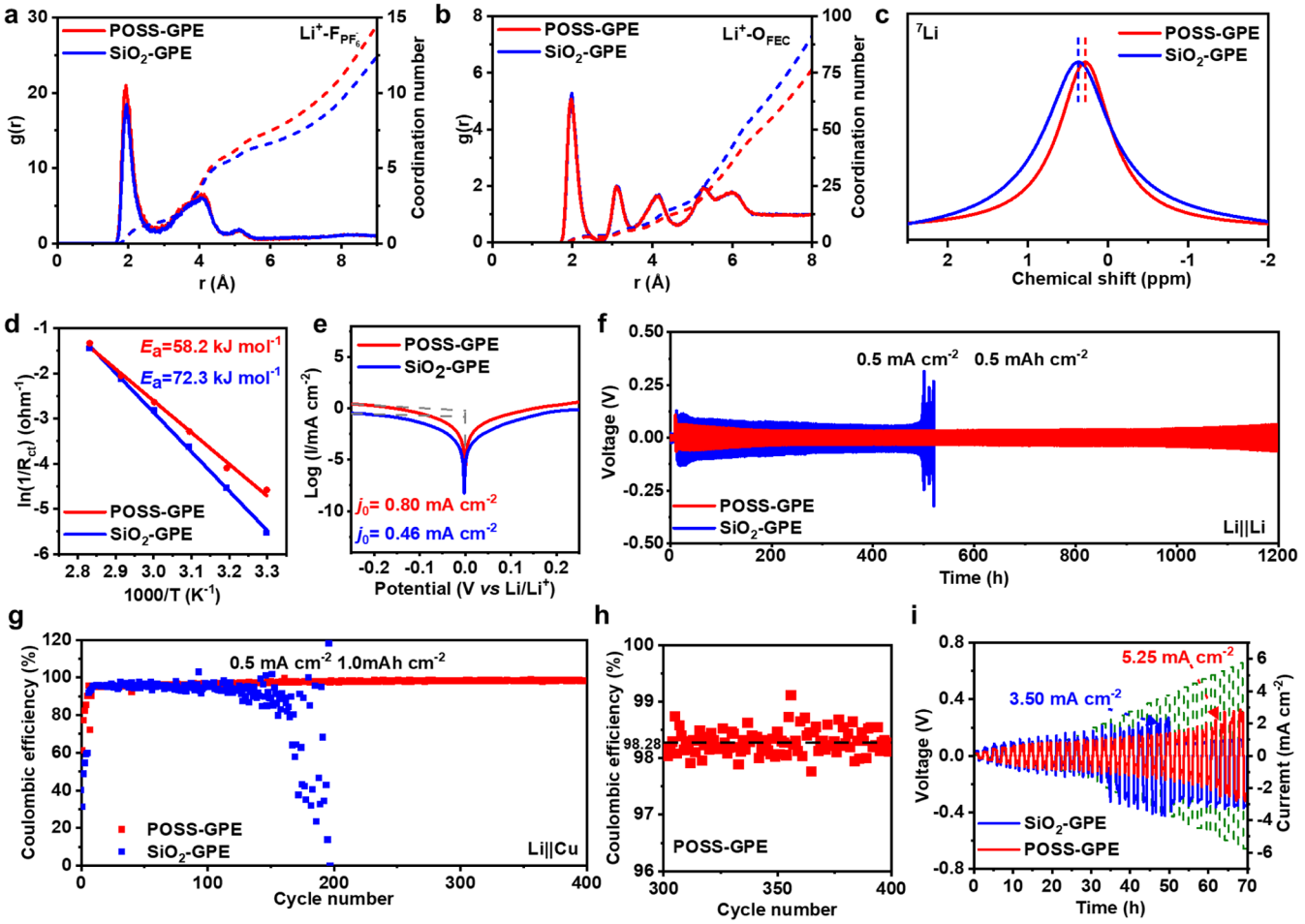


**Figure 1.** The solvation structure characterization and interfacial stability of GPEs with LMAs. The RDF and CN plots of (a) $Li^+$-$F_{PF_6^-}$ and (b) $Li^+$-$O_{FEC}$ pairs calculated by MD simulations. (c) $^7Li$ NMR spectra of POSS-GPE and $SiO_2$-GPE. (d) Activation energies of the $Li^+$ desolvation process calculated by EIS. (e) Tafel plots of Li||Li symmetric cells with POSS-GPE and $SiO_2$-GPE. (f) Cycling performance of Li||Li symmetric cells with POSS-GPE and $SiO_2$-GPE at a current density of 0.5 mA $cm^{-2}$ and a capacity of 0.5 mAh $cm^{-2}$ at 25 °C. (g) Coulombic efficiency of Li||Cu cells with different electrolytes at a current density of 0.5 mA $cm^{-2}$ and a capacity of 1 mAh $cm^{-2}$ at 25 °C. (h) Enlarged view of the Coulombic efficiency of Li||Cu cells with POSS-GPE in Figure 1g from the 301st cycle to 400th cycle. (i) CCD tests of Li||Li symmetric cells with POSS-GPE and $SiO_2$-GPE at 25 °C.

results demonstrate the ability of POSS units to modulate an anion-rich solvation structure (Scheme 1).

## Electrochemical Performance and Solvation Structure Characterization

The ionic conductivities of both POSS-GPE and $SiO_2$-GPE are evaluated across the temperature range from 298 to 353 K (Figure S8). POSS-GPE exhibits high ionic conductivity over the entire range (3.04 mS $cm^{-1}$ at room temperature) and a low activation energy for ionic migration (11.0 kJ $mol^{-1}$). Crucially, the nearly identical conductivities of the two GPEs indicate that the unique interactions of the POSS units do not impede $Li^+$ transport. Furthermore, as shown in Figure S9, electrochemical floating analyses further confirm the excellent oxidation stability of both GPEs, withstanding voltages of up to 4.9 V vs $Li^+$/Li, indicating their stability under high voltages.

To verify the influence of POSS units on the modulation of the solvation structure, the coordination environment of $Li^+$ in both electrolytes is analyzed by molecular dynamics (MD) simulations (Figure S10a-d). The calculated radial distribution function (RDF) and coordination number (CN) are displayed in Figures 1a-b and S10e-f. Notably, POSS-GPE demonstrates a higher CN for $Li^+$-$F_{PF_6^-}$ and a lower CN for $Li^+$-$O_{FEC}$ compared to $SiO_2$-GPE. This result confirms that anions preferentially coordinate with $Li^+$, displacing solvent molecules from the primary solvation sheath and creating the intended anion-rich solvation structure. The simulated solvation structures are then validated experimentally. In $^7Li$ NMR spectra (Figure 1c), the chemical shift of the POSS-GPE reveals an upfield chemical shift (0.286 ppm) compared to the $SiO_2$-GPE (0.371 ppm), suggesting a stronger shielding effect and enhanced $Li^+$−anion interactions.[33] This conclusion is further corroborated by Raman spectra, which reveal a higher proportion of contact ion pairs (CIPs) and reduced solvated FEC molecules in the primary solvation sheath of $Li^+$ within the POSS-GPE (Figure S11).[34] The modulated anion-rich solvation structure with weakened $Li^+$−solvent interactions facilitates the desolvation process of $Li^+$ and promotes the formation of a more stable, inorganic-rich SEI.[35]

Furthermore, electrochemical impedance spectroscopy (EIS) is conducted on Li||Li symmetric cells to probe the desolvation kinetics. Arrhenius fitting of the temperature-dependent EIS data demonstrates a significantly lower


https://doi.org/10.1021/jacs.5c17294
J. Am. Chem. Soc. 2026, 148, 2471−2480

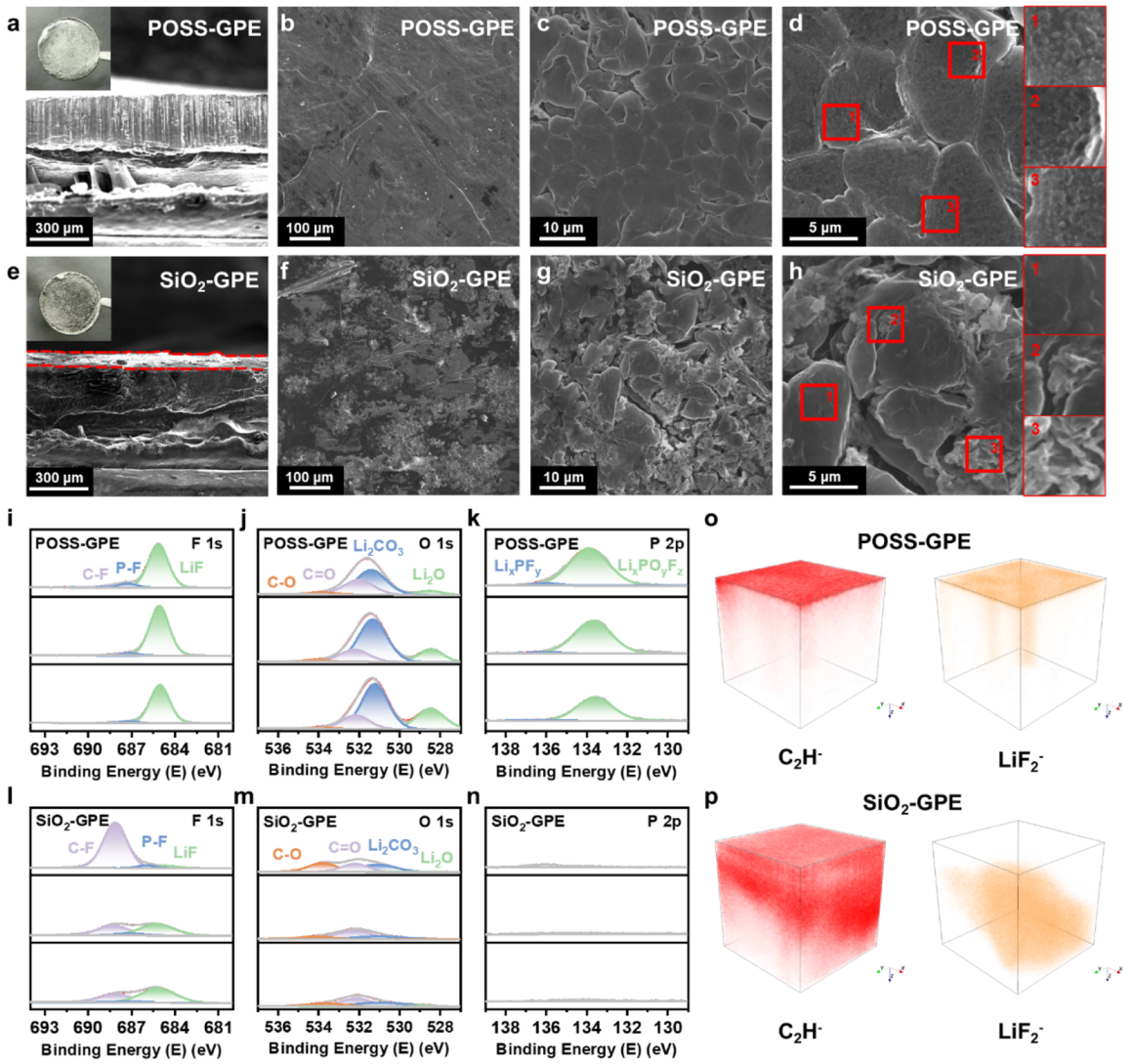


**Figure 2.** The characterization of the SEI. SEM images of cycled Li in Li||Li symmetric cells after 50 cycles with (a-d) POSS-GPE and (e-h) $SiO_2$-GPE at a current density of 0.1 mA $cm^{-2}$ and a capacity of 0.1 mAh $cm^{-2}$ at 25 °C. (i, l) F 1s, (j, m) O 1s, and (k, n) P 2p XPS profiles of the cycled Li in Li||Li symmetric cells with (i-k) POSS-GPE and (l-n) $SiO_2$-GPE after 50 cycles at a current density of 0.1 mA $cm^{-2}$ and a capacity of 0.1 mAh $cm^{-2}$ at 25 °C. ToF-SIMS 3D distribution of $C_2H^-$ and $LiF_2^-$ fragments of the cycled Li in Li||Li symmetric cells with (o) POSS-GPE and (p) $SiO_2$-GPE after 50 cycles at a current density of 0.1 mA $cm^{-2}$ and a capacity of 0.1 mAh $cm^{-2}$.

activation energy ($E_a$) of desolvation for the POSS-GPE (−58.2 kJ $mol^{-1}$) compared to the $SiO_2$-GPE (−72.3 kJ $mol^{-1}$) (Figures 1d and S12).[36] The lower $E_a$ indicates a more facile desolvation process for $Li^+$, which accelerates interfacial charge transfer.[18] This assessment is corroborated by a Tafel analysis (Figure 1e). POSS-GPE exhibits a substantially higher exchange current density ($j_0$) (0.80 mA $cm^{-2}$) compared to the $SiO_2$-GPE (0.46 mA $cm^{-2}$), indicating improved interfacial kinetics, which is conducive to uniform Li deposition.[37]

Owing to the modulated anion-rich solvation structure and improved interfacial kinetics at the surface of LMAs, the POSS-GPE exhibits enhanced reductive stability and lithium compatibility. The cyclic voltammetry (CV) tests on Li||Cu cells confirm the excellent stability, as POSS-GPE shows no obvious reduction peaks down to 0 V vs $Li^+$/Li (Figure S13). In sharp contrast, $SiO_2$-GPE presents a clear reduction peak at 0.7 V vs $Li^+$/Li. This peak is attributed to the solvent decomposition, which leads to an organic-rich SEI.[38] Moreover, Li||Li symmetric cells assembled with POSS-GPE demonstrate excellent stability during Li plating/stripping. The cell maintains a low and stable overpotential for over 1200 h at a current density of 0.5 mA $cm^{-2}$ with an areal capacity of 0.5 mAh $cm^{-2}$. In contrast, the control cell with $SiO_2$-GPE exhibits a higher overpotential and fails within 500 h under the same conditions (Figure 1f). The cycling stability of Li||Li symmetric cells with POSS-GPE is further demonstrated under harsher conditions, sustaining stable cycling for 500 h at a current density of 1 mA $cm^{-2}$ and a capacity of 1 mAh $cm^{-2}$ (Figure S14).

The compatibility of POSS-GPE with LMAs is further quantified by Coulombic efficiency (CE) measurements in Li||Cu cells. At a current density of 0.5 mA $cm^{-2}$ and a capacity of 1 mAh $cm^{-2}$, the Li||Cu cell assembled with POSS-GPE delivers a high average CE of 98.28% (from 301st cycle to 400th cycle). In contrast, the cell with $SiO_2$-GPE suffers from rapid CE degradation, failing at about the 200th cycle with a much lower average CE of 94.14% (from 51st cycle to 150th cycle) (Figure 1g-h). Moreover, the POSS-GPE enables a


https://doi.org/10.1021/jacs.5c17294
J. Am. Chem. Soc. 2026, 148, 2471−2480

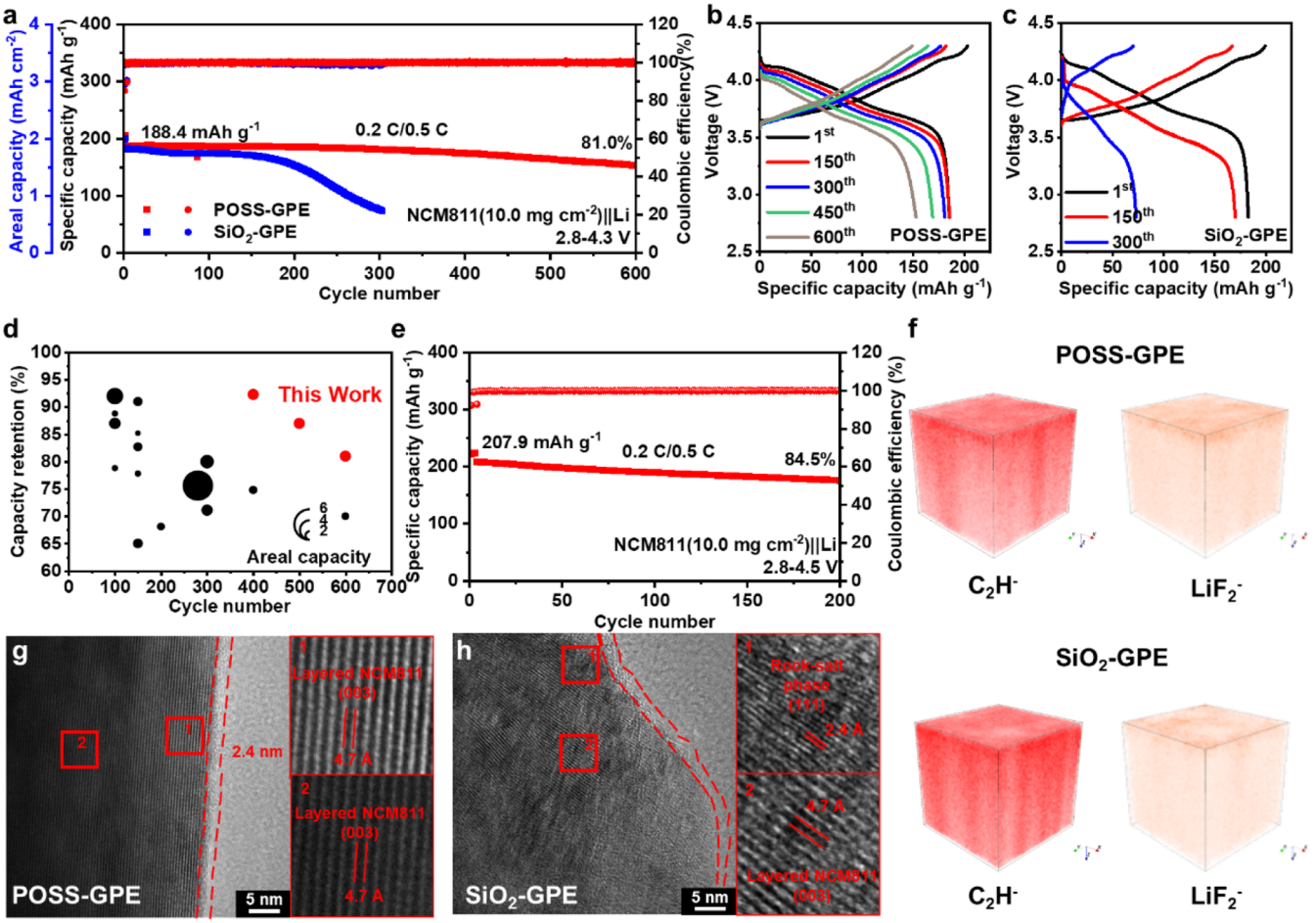


**Figure 3.** Electrochemical performance of high-voltage LMBs and the characterization of the CEI. (a) Long-cycling performance of NCM811||Li batteries with POSS-GPE and $SiO_2$-GPE in the voltage range of 2.8−4.3 V at 25 °C under 0.2 C charge and 0.5 C discharge. Typical charge−discharge curves of NCM811||Li batteries with (b) POSS-GPE, (c) $SiO_2$-GPE in the voltage range of 2.8−4.3 V at 25 °C under 0.2 C charge and 0.5 C discharge. (d) Comparison of the cycling performance of polymer-based LMBs with high-mass-loading NCM cathodes under a cutoff voltage of 4.3 V with literature reports. (e) Long-cycling performance of NCM811||Li batteries with POSS-GPE in the voltage range of 2.8−4.5 V at 25 °C under 0.2 C charge and 0.5 C discharge. (f) ToF-SIMS 3D distribution of $C_2H^-$ and $LiF_2^-$ fragments of the cycled NCM811 cathodes in NCM811||Li batteries after 30 cycles with POSS-GPE and $SiO_2$-GPE in the voltage range of 2.8−4.3 V at 25 °C under 0.2 C charge and 0.5 C discharge. TEM images of cycled NCM811 cathodes in NCM811||Li batteries after 30 cycles with (g) POSS-GPE and (h) $SiO_2$-GPE in the voltage range of 2.8−4.3 V at 25 °C under 0.2 C charge and 0.5 C discharge.

critical current density (CCD) of 5.25 mA $cm^{-2}$, significantly higher than the 3.50 mA $cm^{-2}$ for $SiO_2$-GPE (Figure 1i). Rate performance of Li||Li symmetric cells from 0.1 to 3 mA $cm^{-2}$ further confirms this superiority (Figure S15). The POSS-GPE-based Li||Li symmetric cell displays lower overpotentials at each current density, demonstrating faster Li plating/stripping kinetics.[39] These results collectively demonstrate that the modulated anion-rich solvation structure in the POSS-GPE endows outstanding stability with LMAs, surpassing that of the control, the $SiO_2$-GPE.

## Electrochemical Performance and Characterization of Electrode−Electrolyte Interphase

To elucidate the influence of solvation structure on the interfacial chemistry between the electrolytes and LMAs, comprehensive analyses of cycled anodes are conducted using scanning electron microscopy (SEM), X-ray photoelectron spectroscopy (XPS), and time-of-flight secondary ion mass spectrometry (ToF-SIMS). On the surface of Li cycled in the POSS-GPE system, Li deposits smoothly and densely, forming a uniform submicrometer-sized spherical morphology with no evidence of dendritic growth after 50 cycles (Figure 2a-d). This morphology is considered ideal due to the smooth surface and the reduced reactive area between the LMA and the electrolyte.[40] This desirable outcome is attributed to the formation of a robust SEI and rapid $Li^+$ diffusion kinetics across the interface. In sharp contrast, the surface of cycled Li using $SiO_2$-GPE exhibits a loose, porous structure dominated by dendritic and mossy Li (Figure 2e-h), indicating poor interfacial stability and severe parasitic reactions.

XPS analysis is performed to investigate the chemical composition and depth profile of the SEI (Figures 2i-n and S16). In the POSS-GPE system, the F 1s and P 2p spectra of cycled Li show intense and depth-homogeneous signals corresponding to LiF and $Li_xPO_yF_z$, which are decomposition products of the $PF_6^-$ anion.[41,42] A prominent $Li_2O$ peak is observed in the SEI formed on cycled Li within the POSS-GPE system, which facilitates $Li^+$ diffusion through the SEI.[43,44] These results confirm the formation of an inorganic-rich SEI driven by an anion-rich solvation structure. In contrast, signals from organic species (such as C═O, $RCO_2Li$ and $-CF_x$), originating from solvent and polymer decomposition, are


https://doi.org/10.1021/jacs.5c17294
J. Am. Chem. Soc. 2026, 148, 2471−2480

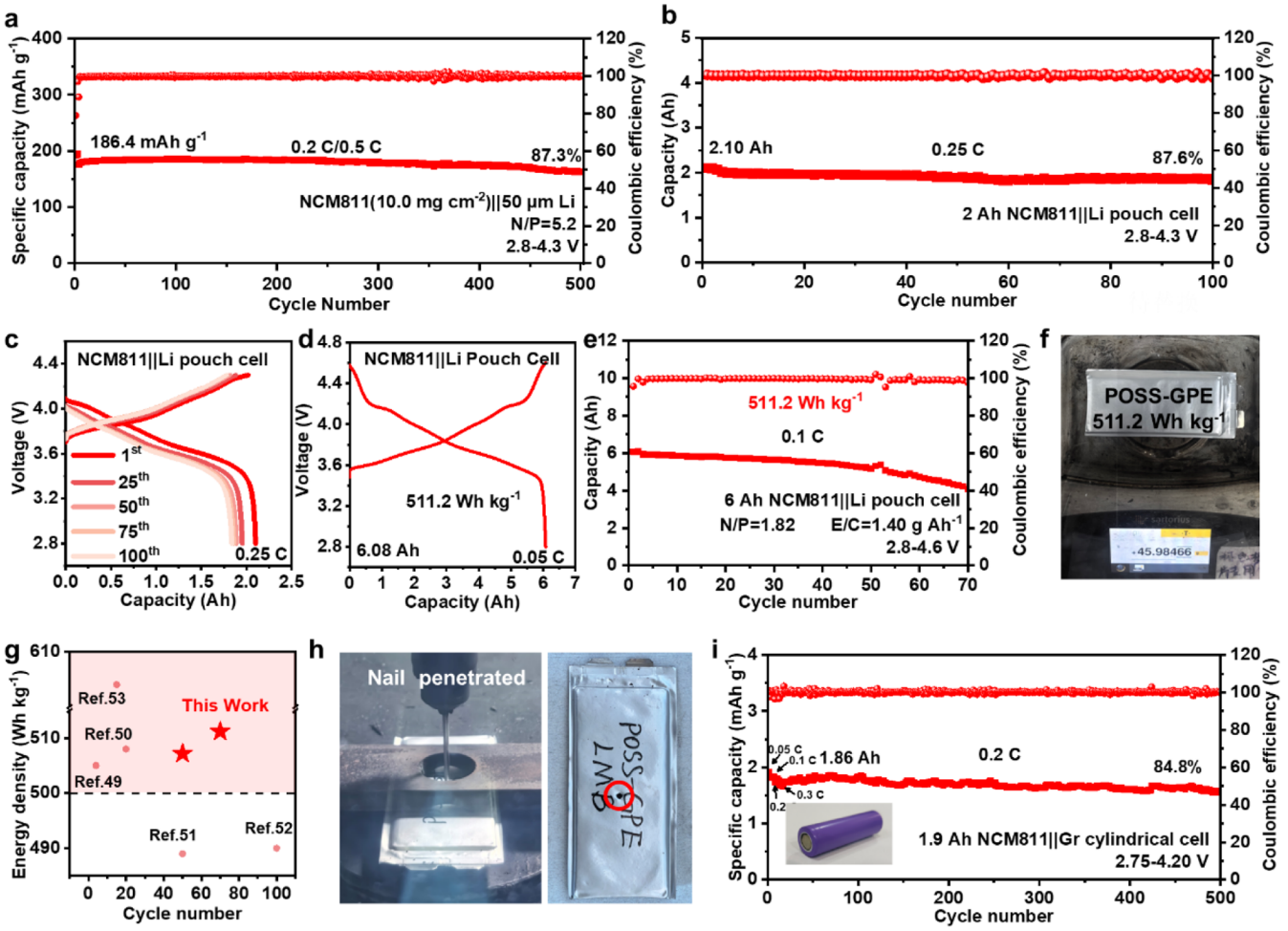


**Figure 4.** Electrochemical and safety performance of full cells and practical cells. (a) Long-cycling performance of NCM811(10.0 mg $cm^{-2}$)||Li (50 $\mu$m) full cell with POSS-GPE in the voltage range of 2.8−4.3 V at 25 °C under 0.2 C charge and 0.5 C discharge. (b) Cycling performance and (c) typical charge−discharge curves of 2 Ah NCM811|POSS-GPE|Li pouch cell in the voltage range of 2.8−4.3 V at 25 °C under 0.25 C. (d) Typical charge−discharge curve, (e) cycling performance, (f) photograph of 6.08 Ah NCM811|POSS-GPE|Li in the voltage range of 2.8−4.6 V at 25 °C under 0.1 C. (g) Comparison of energy density and cycling performance of polymer-based pouch cells with literature reports. (h) Nail test of NCM811|POSS-GPE|Li pouch cell. (i) Cycling performance of the 1.9 Ah NCM811|POSS-GPE|Gr cylindrical cell in the voltage range of 2.75−4.20 V at 25 °C under 0.2 C.

significantly suppressed. Conversely, the SEI formed on cycled Li in the $SiO_2$-GPE system is dominated by organic species, with only minor inorganic products originating from anion reduction.[45]

Furthermore, ToF-SIMS is employed to visualize the three-dimensional (3D) distribution of SEI components (Figure 2o-p). The result reveals a thin and uniform SEI forming on the cycled LMA using the POSS-GPE. In contrast, the cycled LMA using the $SiO_2$-GPE exhibits a thick and uneven distribution of both LiF and organic species, indicating extensive electrolyte decomposition and a nonuniform and unstable SEI.[46] Overall, these multitechnique characterizations provide compelling evidence that the POSS-GPE promotes the formation of a stable, uniform, and inorganic-rich SEI. This superior interphase underpins the enhanced electrochemical performance.

Given its exceptional oxidation stability and ability to form a robust SEI, the POSS-GPE is expected to enable outstanding electrochemical performance in high-voltage LMBs. To validate this hypothesis, we assemble full cells employing commercial high-mass-loading NCM811 cathodes (10.0 mg $cm^{-2}$). As shown in Figure 3a-c, the NCM811|POSS-GPE|Li cell delivers a high specific capacity of 188.4 mAh $g^{-1}$ and maintains 81.0% of its capacity after 600 cycles. This result matches the state-of-the-art performance for polymer electrolyte-based LMBs (Figure 3d and Table S1). In sharp contrast, the control NCM811|$SiO_2$-GPE|Li cell shows a significantly shorter cycle life. Additionally, EIS measurements are carried out to investigate the kinetics of the electrochemical process.[47] As shown in Figure S17, after 10 cycles, the NCM811||Li battery assembled with POSS-GPE exhibits significantly lower charge transfer resistance ($R_{ct}$) and surface film resistance ($R_{sf}$) compared to the control $SiO_2$-GPE system. This result demonstrates the formation of a more conductive and stable electrode−electrolyte interphase within the POSS-GPE system.[48] The stability of POSS-GPE is further demonstrated by the excellent cycling performance of NCM811|POSS-GPE|Li cells at elevated operating voltages ranging from 4.5 to 4.7 V (Figures 3e and S18). The POSS-GPE exhibits outstanding compatibility with other high-voltage cathode materials, including Li-rich $Li_{1.2}Ni_{0.13}Co_{0.13}Mn_{0.54}O_2$ (LNCMO, 7.6 mg $cm^{-2}$, stably cycle at 4.7 V) and high-voltage spinel


https://doi.org/10.1021/jacs.5c17294
J. Am. Chem. Soc. 2026, 148, 2471−2480

$LiNi_{0.5}Mn_{1.5}O_4$ (LNMO, 8.8 mg $cm^{-2}$, stably cycle up to 4.9 V), underscoring its exceptional oxidative stability (Figures S19−S20). Furthermore, the NCM811|POSS-GPE|Li battery demonstrates excellent rate performance, delivering high discharge capacities of 205.9, 196.4, 184.1, 173.0 mAh $g^{-1}$ at 0.1, 0.2, 0.5, and 1 C, respectively, which significantly outperforms the $SiO_2$-GPE-based cell (159.0 mAh $g^{-1}$ at 1 C) (Figure S21). These results highlight the enhanced interfacial kinetics.

To elucidate the origin of the exceptional cycling stability and rate performance enabled by the POSS-GPE, XPS depth profiling is conducted to analyze the composition of CEI on cycled NCM811 cathodes (Figure S22). The resulting depth profiling indicates a predominantly inorganic CEI formed on the cycled NCM811 cathode using the POSS-GPE, evidenced by a higher LiF signal and a lower C═O signal (originating from organic decomposition) compared to the control $SiO_2$-GPE. This result is further supported by ToF-SIMS analysis (Figures 3f and S23), which reveals a higher concentration of LiF and a lower intensity of organic fragments ($C_2H^-$) in the CEI of the cycled NCM811 cathode using the POSS-GPE. The morphology of the CEI ofthe cycled NCM811 cathode in the POSS-GPE system is further examined by transmission electron microscope (TEM) (Figure 3g-h), revealing a uniform CEI with a thickness of approximately 2.4 nm on the surface of NCM811. Critically, the layered structure of NCM811 is well preserved from the surface to the bulk, confirming that the inorganic-rich CEI effectively protects the cathode from parasitic reactions and structural degradation at high voltages. In sharp contrast, the nonuniform CEI formed on the surface of the NCM811 cathode in the control $SiO_2$-GPE system fails to provide adequate protection, leading to severe surface reconstruction and the formation of a rock-salt phase after cycling at high voltage.

### Electrochemical Performance and Safety Tests of Practical Cells

To bridge the gap between laboratory research and real-world applications, the performance of the POSS-GPE is systematically evaluated in a series of practical battery configurations under challenging conditions. Full cells with low N/P ratios are assembled with high-mass-loading NCM811 cathodes (10.0 and 21.5 mg $cm^{-2}$) and thin Li foil (50 $\mu$m). The NCM811|POSS-GPE|Li full cell with an N/P ratio of 5.2 delivers stable cycling with 87.3% capacity retained after 500 cycles (Figure 4a). Even under a lower N/P ratio of 2.5, the NCM811|POSS-GPE|Li full cell still exhibits excellent cycling performance with a capacity retention of 87.3% after 150 cycles, significantly outperforming the control $SiO_2$-GPE-based full cell (Figure S24a). Moreover, POSS-GPE can support the stable operation of the full cell with a higher cathode loading of 46.2 mg $cm^{-2}$ and a lower N/P ratio of 1.1, as shown in Figure S24b.[22] In addition to their attractive electrochemical performance at room temperature, POSS-GPE-based LMBs demonstrate excellent cycling stability at harsh temperatures (Figure S25). At a low temperature of 0 °C, POSS-GPE exhibits a high ionic conductivity of 1.5 mS $cm^{-1}$. As a result, the high-mass-loading NCM811 (10.0 mg $cm^{-2}$)|POSS-GPE|Li battery delivers a high discharge capacity of 213.5 mAh $g^{-1}$ with stable cycling performance. POSS-GPE also demonstrates excellent electrochemical stability at high temperature, enabling stable operation at 60 °C. This wide temperature tolerance further confirms the practical application prospects of POSS-GPE.

Furthermore, scaled-up high-voltage pouch cells are assembled and evaluated. A 2-Ah NCM811|POSS-GPE|Li pouch cell achieves a cycle life of 100 cycles with 87.6% capacity retention at 4.3 V (Figure 4b-c). The remarkable energy density of 507.2 Wh $kg^{-1}$ is successfully achieved in a 5.97-Ah NCM811|POSS-GPE|Li pouch cell operated with a lean electrolyte content (E/C = 1.26 g $Ah^{-1}$) and a high voltage of 4.6 V. This pouch cell demonstrates a cycle life of 50 cycles with 87.4% capacity retention (Figure S26 and Table S2). By optimizing the E/C ratio to 1.40 g $Ah^{-1}$, both discharge capacity and average discharge voltage are enhanced due to the improved electrode infiltration and reduced polarization. As a result, a superior energy density of 511.2 Wh $kg^{-1}$ is achieved, along with an extended cycle life of 70 cycles (Figure 4d-f and Table S2). These results indicate that POSS-GPE achieves the best balance between energy density and cycling performance for polymer-electrolyte-based LMBs (Figure 4g and Table S3).[49−53] Moreover, the high-energy-density pouch cells also demonstrate exceptional safety by passing the rigorous nail-penetration test without any electrolyte leakage, ignition, or combustion (Figure 4h).

Finally, to demonstrate the versatility and commercial viability of POSS-GPE, industrial-standard solid-state 18650 cylindrical cells are fabricated. An NCM811|POSS-GPE|graphite (Gr) cylindrical cell exhibits excellent rate and cycling performance, retaining 84.8% capacity after 500 cycles (Figure 4i and Table S4). Moreover, a 3.3 Ah cylindrical cell using a Si/C anode also delivers high capacity and stable cycling over 100 cycles (Figure S27 and Table S5), confirming the excellent compatibility of POSS-GPE with commercial anode materials. The outstanding electrochemical performance and safety of both high-energy density pouch cells and industry-standard 18650 cylindrical cells effectively support the practical application potential of POSS-GPE in next-generation high-energy lithium batteries.

## CONCLUSION

In summary, a POSS-GPE has been successfully developed by *in situ* polymerization to improve the cycling performance and safety of high-energy-density LMBs. The POSS-GPE exhibits a high ionic conductivity of 3.04 mS $cm^{-1}$ at room temperature, excellent oxidative stability up to 4.9 V vs $Li^+/Li$, and flame retardancy. The excellent performance of POSS-GPE arises from the ability of POSS units to engineer a desirable anion-rich solvation structure, which promotes the formation of robust, inorganic-rich SEI and CEI layers, thereby improving cycling stability. Consequently, POSS-GPE enables the full cell of NCM811|POSS-GPE|Li (50 $\mu$m) to achieve a long cycle life of 500 cycles, retaining 87.3% capacity. More importantly, an excellent energy density of 511.2 Wh $kg^{-1}$ is achieved in a 6.08 Ah POSS-GPE-based pouch cell (E/C = 1.40 g $Ah^{-1}$), which delivers stable cycling for 70 cycles under a high operating voltage of 4.6 V, representing the best balance between cycling performance and energy density for polymer−electrolyte-based LMBs. Therefore, this work demonstrates that high-energy-density and high-safety solid-state LMBs can be achieved through our polymer matrix strategy to modulate the solvation structure in electrolyte systems.


https://doi.org/10.1021/jacs.5c17294
J. Am. Chem. Soc. 2026, 148, 2471−2480

## ■ ASSOCIATED CONTENT

### Supporting Information

The Supporting Information is available free of charge at https://pubs.acs.org/doi/10.1021/jacs.5c17294.

Including preparation of GPEs; fabrication of batteries; DFT calculations and MD simulations; IR, Raman, and XPS spectra; Photographs of precursors and GPEs; tensile tests; ignition tests; EIS; electrochemical floating analysis; CV; electrochemical performance of Li||Li symmetric cells, half cells, full cells, pouch cells, and 18 650 cylindrical cells; additional tables (PDF)

Video S1: The nail-penetration test of POSS-GPE-based NCM811||Li pouch cell (MP4)

## ■ AUTHOR INFORMATION


### Corresponding Authors

**Yongsheng Chen** − *The Centre of Nanoscale Science and Technology and Key Laboratory of Functional Polymer Materials, Institute of Polymer Chemistry, College of Chemistry, Nankai University, Tianjin 300071, China; State Key Laboratory of Elemento-Organic Chemistry, Renewable Energy Conversion and Storage Center (RECAST), and Frontiers Science Center for New Organic Matter, Nankai University, Tianjin 300071, China;* orcid.org/0000-0003-1448-8177; Email: yschen99@nankai.edu.cn

**Hongtao Zhang** − *The Centre of Nanoscale Science and Technology and Key Laboratory of Functional Polymer Materials, Institute of Polymer Chemistry, College of Chemistry, Nankai University, Tianjin 300071, China; Renewable Energy Conversion and Storage Center (RECAST) and Frontiers Science Center for New Organic Matter, Nankai University, Tianjin 300071, China;* Email: htzhang@nankai.edu.cn

### Authors

**Nuo Xu** − *The Centre of Nanoscale Science and Technology and Key Laboratory of Functional Polymer Materials, Institute of Polymer Chemistry, College of Chemistry, Nankai University, Tianjin 300071, China; Renewable Energy Conversion and Storage Center (RECAST) and Frontiers Science Center for New Organic Matter, Nankai University, Tianjin 300071, China*

**Xingchen Song** − *The Centre of Nanoscale Science and Technology and Key Laboratory of Functional Polymer Materials, Institute of Polymer Chemistry, College of Chemistry, Nankai University, Tianjin 300071, China; Renewable Energy Conversion and Storage Center (RECAST) and Frontiers Science Center for New Organic Matter, Nankai University, Tianjin 300071, China*

**Guolin Sun** − *The Centre of Nanoscale Science and Technology and Key Laboratory of Functional Polymer Materials, Institute of Polymer Chemistry, College of Chemistry, Nankai University, Tianjin 300071, China; Renewable Energy Conversion and Storage Center (RECAST) and Frontiers Science Center for New Organic Matter, Nankai University, Tianjin 300071, China*

**Jinping Zhang** − *The Centre of Nanoscale Science and Technology and Key Laboratory of Functional Polymer Materials, Institute of Polymer Chemistry, College of Chemistry, Nankai University, Tianjin 300071, China; Renewable Energy Conversion and Storage Center (RECAST) and Frontiers Science Center for New Organic Matter, Nankai University, Tianjin 300071, China*

**Zuhao Quan** − *The Centre of Nanoscale Science and Technology and Key Laboratory of Functional Polymer Materials, Institute of Polymer Chemistry, College of Chemistry, Nankai University, Tianjin 300071, China; Renewable Energy Conversion and Storage Center (RECAST) and Frontiers Science Center for New Organic Matter, Nankai University, Tianjin 300071, China*

**Genglin Lou** − *Tianjin Plannano Technology Company Limited, Tianjin 300071, China*

**Aihong Li** − *Tianjin Plannano Technology Company Limited, Tianjin 300071, China*

**Chenxi Li** − *The Centre of Nanoscale Science and Technology and Key Laboratory of Functional Polymer Materials, Institute of Polymer Chemistry, College of Chemistry, Nankai University, Tianjin 300071, China; Renewable Energy Conversion and Storage Center (RECAST) and Frontiers Science Center for New Organic Matter, Nankai University, Tianjin 300071, China*

Complete contact information is available at: https://pubs.acs.org/10.1021/jacs.5c17294


### Notes

The authors declare no competing financial interest.

## ■ ACKNOWLEDGMENTS

The authors gratefully acknowledge the financial support from the National Key R&D Program of China (2020YFA0711500), the National Natural Science Foundation of China (NSFC, 52090034), Beijing−Tianjin−Hebei Basic Research Cooperation project (B2024408025), and the Natural Science Foundation of Tianjin (24JCZXJC00360).

## ■ REFERENCES


(1) Kim, M. S.; Zhang, Z.; Rudnicki, P. E.; Yu, Z.; Wang, J.; Wang, H.; Oyakhire, S. T.; Chen, Y.; Kim, S. C.; Zhang, W.; Boyle, D. T.; Kong, X.; Xu, R.; Huang, Z.; Huang, W.; Bent, S. F.; Wang, L.; Qin, J.; Bao, Z.; Cui, Y. Suspension electrolyte with modified Li+ solvation environment for lithium metal batteries. *Nat. Mater.* **2022**, *21*, 445−454.

(2) Zhu, J.; Bian, P.; Sun, G.; Zhang, J.; Lou, G.; Song, X.; Zhao, R.; Liu, J.; Xu, N.; Li, A.; et al. Practical High-Voltage Lithium Metal Batteries Enabled by the In-Situ Fabrication of Main-Chain Fluorinated Polymer Electrolytes. *Angew. Chem., Int. Ed.* **2025**, *64*, No. e202424685.

(3) Liu, J.; Bao, Z.; Cui, Y.; Dufek, E. J.; Goodenough, J. B.; Khalifah, P.; Li, Q.; Liaw, B. Y.; Liu, P.; Manthiram, A.; Meng, Y. S.; Subramanian, V. R.; Toney, M. F.; Viswanathan, V. V.; Whittingham, M. S.; Xiao, J.; Xu, W.; Yang, J.; Yang, X.; Zhang, J. Pathways for practical high-energy long-cycling lithium metal batteries. *Nat. Energy* **2019**, *4*, 180−186.

(4) Shen, Y.; Li, T.; Ren, K.; Yuan, S.; Ding, K.; Xia, K.; Bao, J. L.; Wang, Y. Integrating Ethereal Molecular Backbones into the Ester Solvent with High Solubility of Nitrate for High-Voltage Li Metal Batteries. *Adv. Mater.* **2025**, *37*, 2501654.

(5) Wang, H.; Yang, J.; Xu, X.; Geng, J.; Lin, X.; Xu, H.; Huang, Y. Competitive Ion Coordination in Gel Polymer Electrolytes Enables Decoupling of Mechanical Strength and Ionic Conductivity. *Adv. Mater.* **2025**, *37*, No. e04625.

(6) Xiong, Q.; Li, D.; Li, S.; Zhang, D.; Li, R.; Zhang, S.; Wang, S.; Hong, H.; Zhu, D.; Liu, Q.; et al. A practical 4.8-V Li||$LiCoO_2$ battery. *Sci. Adv.* **2025**, *11*, No. eadx5020.

(7) He, X.; Zhang, K.; Zhu, Z.; Tong, Z.; Liang, X. 3D-hosted lithium metal anodes. *Chem. Soc. Rev.* **2024**, *53*, 9−24.

(8) Zhang, G.; Li, J.; Chi, S.-S.; Wang, J.; Wang, Q.; Ke, R.; Liu, Z.; Wang, H.; Wang, C.; Chang, J.; et al. Molecular Design of Competitive Solvation Electrolytes for Practical High-Energy and Long-Cycling Lithium-Metal Batteries. *Adv. Funct. Mater.* **2024**, *34*, 2312413.
(9) Kim, J.; Lee, D. G.; Lee, J. H.; Kim, S.; Park, C.-Y.; Lee, J.; Kwon, H.; Cho, H.; Lee, J.; Son, D.; Kim, H.-T.; Choi, N.-S.; Lee, T. K.; Lee, J. Concurrent electrode-electrolyte interfaces engineering via nano-$Si_3N_4$ additive for high-rate, high-voltage lithium metal batteries. *Energy Environ. Sci.* **2025**, *18*, 3148−3159.
(10) Zhao, Q.; Liu, X.; Stalin, S.; Khan, K.; Archer, L. A. Solid-state polymer electrolytes with in-built fast interfacial transport for secondary lithium batteries. *Nat. Energy* **2019**, *4*, 365−373.
(11) Chen, R.; Li, Q.; Yu, X.; Chen, L.; Li, H. Approaching Practically Accessible Solid-State Batteries: Stability Issues Related to Solid Electrolytes and Interfaces. *Chem. Rev.* **2020**, *120*, 6820−6877.
(12) Zhang, Q.; Liu, K.; Ding, F.; Liu, X. Recent advances in solid polymer electrolytes for lithium batteries. *Nano Res.* **2017**, *10*, 4139−4174.
(13) Cheng, X.; Pan, J.; Zhao, Y.; Liao, M.; Peng, H. Gel Polymer Electrolytes for Electrochemical Energy Storage. *Adv. Energy Mater.* **2018**, *8*, 1702184.
(14) Xu, N.; Zhao, Y.; Ni, M.; Zhu, J.; Song, X.; Bi, X.; Zhang, J.; Zhang, H.; Ma, Y.; Li, C.; et al. In-Situ Cross-linked F- and P-Containing Solid Polymer Electrolyte for Long-Cycling and High-Safety Lithium Metal Batteries with Various Cathode Materials. *Angew. Chem., Int. Ed.* **2024**, *63*, No. e202404400.
(15) Song, Z.; Chen, F.; Martinez-Ibañez, M.; Feng, W.; Forsyth, M.; Zhou, Z.; Armand, M.; Zhang, H. A reflection on polymer electrolytes for solid-state lithium metal batteries. *Nat. Commun.* **2023**, *14*, 4884.
(16) Zhou, D.; Shanmukaraj, D.; Tkacheva, A.; Armand, M.; Wang, G. Polymer Electrolytes for Lithium-Based Batteries: Advances and Prospects. *Chem* **2019**, *5*, 2326−2352.
(17) Wu, S.; Liu, X.; Hao, Z.; Sun, X.; Hou, J.; Shang, L.; Wang, L.; Zhang, K.; Li, H.; Yan, Z.; Chen, J. Uncovering the Crucial Role of Chelating Structures in Cyano-AlkylPhosphate Electrolytes for High-Voltage Lithium Metal Batteries. *J. Am. Chem. Soc.* **2024**, *146*, 28770−28782.
(18) Jang, J.; Wang, C.; Kang, G.; Han, C.; Han, J.; Shin, J.-S.; Ko, S.; Kim, G.; Baek, J.; Kim, H.-T.; Lee, H.; Park, C. B.; Seo, D.-H.; Li, Y.; Kang, J. Miniature $Li^+$ solvation by symmetric molecular design for practical and safe Li-metal batteries. *Nat. Energy* **2025**, *10*, 502−512.
(19) Cui, Z.; Jia, Z.; Ruan, D.; Nian, Q.; Fan, J. F.; Chen, S.; He, Z.; Wang, D.; Jiang, J.; Ma, J.; et al. Molecular anchoring of free solvents for high-voltage and high-safety lithium metal batteries. *Nat. Commun.* **2024**, *15*, 2033.
(20) Chen, Y.-P.; Niu, Y.-L.; Zheng, Z.; Chen, X.; Gao, Y.-C.; Yao, N.; Zhang, R.; Zhang, Q. The Origin of Anion-Rich Solvation Structures in Siloxane Electrolytes. *Angew. Chem., Int. Ed.* **2025**, *64*, No. e202508152.
(21) Wang, H.; Zhang, X.; Li, Y.; Xu, L.-W. Siloxane-Based Organosilicon Materials in Electrochemical Energy Storage Devices. *Angew. Chem., Int. Ed.* **2022**, *61*, No. e202210851.
(22) Ni, M.; Zhao, Y.; Xu, N.; Kong, M.; Ma, Y.; Li, C.; Zhang, H.; Chen, Y. Improving the cycling stability of lithium-ion batteries with a dry-processed cathode via the synergistic effect of carboxymethyl cellulose and siloxane. *Sci. China Mater.* **2024**, *67*, 76−84.
(23) Wang, Q.; Zhang, H.; Cui, Z.; Zhou, Q.; Shangguan, X.; Tian, S.; Zhou, X.; Cui, G. Siloxane-based polymer electrolytes for solid-state lithium batteries. *Energy Storage Mater.* **2019**, *23*, 466−490.
(24) Tanaka, K.; Chujo, Y. Advanced functional materials based on polyhedral oligomeric silsesquioxane (POSS). *J. Mater. Chem.* **2012**, *22*, 1733−1746.
(25) Chen, X.; Liang, L.; Hu, W.; Liao, H.; Zhang, Y. POSS hybrid poly(ionic liquid) ionogel solid electrolyte for flexible lithium batteries. *J. Power Sources* **2022**, *542*, 231766.
(26) Qiao, G.-Y.; Wang, X.; Li, X.; Li, J.; Geng, K.; Jin, E.; Xu, J.-J.; Yu, J. Unlocking Synthesis of Polyhedral Oligomeric Silsesquioxane-Based Three-Dimensional Polycubane Covalent Organic Frameworks. *J. Am. Chem. Soc.* **2024**, *146*, 3373−3382.
(27) Wang, H.; Chen, S.; Li, Y.; Liu, Y.; Jing, Q.; Liu, X.; Liu, Z.; Zhang, X. Organosilicon-Based Functional Electrolytes for High-Performance Lithium Batteries. *Adv. Energy Mater.* **2021**, *11*, 2101057.
(28) Miao, X.; Hong, J.; Huang, S.; Huang, C.; Liu, Y.; Liu, M.; Zhang, Q.; Jin, H. In Situ Gel Polymer Electrolyte with Rapid $Li^+$ Transport Channels and Anchored Anion Sites for High-Current-Density Lithium-Ion Batteries. *Adv. Funct. Mater.* **2025**, *35*, 2411751.
(29) Xu, W.; Dong, W.; Lin, J.; Mu, K.; Song, Z.; Tan, J.; Wang, R.; Liu, Q.; Zhu, C.; Xu, J.; et al. Optimization Design of Fluoro-Cyanogen Copolymer Electrolyte to Achieve 4.7 V High-Voltage Solid Lithium Metal Battery. *Adv. Sci.* **2024**, *11*, 2400466.
(30) Li, C.; Huang, Y.; Chen, C.; Feng, X.; Zhang, Z.; Liu, P. A high-performance solid electrolyte assisted with hybrid biomaterials for lithium metal batteries. *J. Colloid Interface Sci.* **2022**, *608*, 313−321.
(31) Tan, S.-J.; Yue, J.; Chen, Z.; Feng, X.-X.; Zhang, J.; Yin, Y.; Zhang, L.; Zheng, J.-C.; Luo, Y.; Xin, S.; et al. Asymmetric Fire-Retardant Quasi-Solid Electrolytes for Safe and Stable High-Voltage Lithium Metal Battery. *Energy Mater. Adv.* **2024**, *5*, 0076.
(32) Zhu, J.; Zhang, J.; Zhao, R.; Zhao, Y.; Liu, J.; Xu, N.; Wan, X.; Li, C.; Ma, Y.; Zhang, H.; Chen, Y. In situ 3D crosslinked gel polymer electrolyte for ultra-long cycling, high-voltage, and high-safety lithium metal batteries. *Energy Storage Mater.* **2023**, *57*, 92−101.
(33) Yang, W.; Zhang, Z.; Sun, X.; Liu, Y.; Sheng, C.; Chen, A.; He, P.; Zhou, H. Tailoring the Electrode-Electrolyte Interface for Reliable Operation of All-Climate 4.8 V Li||NCM811 Batteries. *Angew. Chem., Int. Ed.* **2024**, *63*, No. e202410893.
(34) Cheng, H.; Ma, Z.; Kumar, P.; Liang, H.; Cao, Z.; Xie, H.; Cavallo, L.; Kim, H.; Li, Q.; Sun, Y.-K.; et al. High Voltage Electrolyte Design Mediated by Advanced Solvation Chemistry Toward High Energy Density and Fast Charging Lithium-Ion Batteries. *Adv. Energy Mater.* **2024**, *14*, 2304321.
(35) Wu, L.-Q.; Li, Z.; Fan, Z.-Y.; Li, K.; Li, J.; Huang, D.; Li, A.; Yang, Y.; Xie, W.; Zhao, Q. Unveiling the Role of Fluorination in Hexacyclic Coordinated Ether Electrolytes for High-Voltage Lithium Metal Batteries. *J. Am. Chem. Soc.* **2024**, *146*, 5964−5976.
(36) Liang, P.; Hu, H.; Dong, Y.; Wang, Z.; Liu, K.; Ding, G.; Cheng, F. Competitive Coordination of Ternary Anions Enabling Fast Li-Ion Desolvation for Low-Temperature Lithium Metal Batteries. *Adv. Funct. Mater.* **2024**, *34*, 230958.
(37) Fang, S.; Wu, F.; Zhao, S.; Zarrabeitia, M.; Kim, G.-T.; Kim, J.-K.; Zhou, N.; Passerini, S. Adaptive Multi-Site Gradient Adsorption of Siloxane-Based Protective Layers Enable High Performance Lithium-Metal Batteries. *Adv. Energy Mater.* **2023**, *13*, 2302577.
(38) Xu, Z.; Zhang, X.; Yang, J.; Cui, X.; Nuli, Y.; Wang, J. High-voltage and intrinsically safe electrolytes for Li metal batteries. *Nat. Commun.* **2024**, *15*, 9856.
(39) Gu, S.; Zhang, Y.; Li, M.; Lin, Q.; Xu, G.; Zhang, N. Internal Electron-Donation Allocation Design for Intrinsic Solubilization of Lithium Nitrate in Ester Electrolyte for Stable Lithium Metal Batteries. *Angew. Chem., Int. Ed.* **2025**, *64*, No. e202410020.
(40) Chen, X. R.; Yao, Y. X.; Yan, C.; Zhang, R.; Cheng, X. B.; Zhang, Q. A Diffusion–Reaction Competition Mechanism to Tailor Lithium Deposition for Lithium-Metal Batteries. *Angew. Chem., Int. Ed.* **2020**, *59*, 7743−7747.
(41) Ren, Q.; Wang, Q.; Su, L.; Liu, G.; Song, Y.; Shangguan, X.; Li, F. Inorganic/organic composite fluorinated interphase layers for stabilizing ether-based electrolyte in high-voltage lithium metal batteries. *J. Mater. Chem. A* **2024**, *12*, 1072−1080.
(42) Cao, Y.; Li, N.; Yuan, K.; Li, N.; Zhang, W.; Liang, S.; Hou, Z.; Lei, D.; Jin, T.; Wang, J.; Xie, K.; Shen, C. Revealing the mechanisms of electrolyte additive PTS on Ni-rich electrode: Tolerance to high temperature (50 °C) and high voltage (4.6 V). *Energy Storage Mater.* **2023**, *60*, 102851.
(43) Ryu, K.; Lee, K.; Lim, J.; Lee, M. J.; Kim, K.-H.; Lee, U. H.; Rinkel, B.; Kim, K.; Kim, S.; Kim, D.; Shin, D.; McCloskey, B. D.; Kang, J.; Lee, S. W. Additive engineering strategies for improved


https://doi.org/10.1021/jacs.5c17294
J. Am. Chem. Soc. 2026, 148, 2471−2480

interfacial stability in lithium metal batteries. *Energy Environ. Sci.* **2024**, *17*, 7772−7781.
(44) Yuan, Y.; Wu, F.; Liu, Y.; Wang, X.; Zhang, K.; Zheng, L.; Wang, Z.; Bai, Y.; Wu, C. Rational Tuning of a $Li_4SiO_4$-Based Hybrid Interface with Unique Stepwise Prelithiation for Dendrite-Proof and High-Rate Lithium Anodes. *ACS Appl. Mater. Interfaces* **2020**, *12*, 39362−39371.
(45) Liu, J.; Shen, X.; Zhou, J.; Wang, M.; Niu, C.; Qian, T.; Yan, C. Nonflammable and High-Voltage-Tolerated Polymer Electrolyte Achieving High Stability and Safety in 4.9 V-Class Lithium Metal Battery. *ACS Appl. Mater. Interfaces* **2019**, *11*, 45048−45056.
(46) Wu, L.; Li, Z.; Li, H.; Zhang, J.; Li, Y.; Ren, S.; Fan, Z.; Wang, X.; Li, K.; Liu, Z.; Zhang, J.; Yang, J.; Li, Y.; Bo, S.; Zhao, Q. Regulating Amine Substitution in Fluorosulfonyl-Based Flame-Retardant Electrolytes for Energy-Dense Lithium Metal Batteries. *J. Am. Chem. Soc.* **2025**, *147*, 16506−16521.
(47) Li, C.; Wang, W.; Feng, X.; Wang, Y.; Zhang, Y.; Zhang, J.; Zhang, L.; Zheng, J.; Luo, Y.; Chen, Z.; Xin, S.; Guo, Y. High-Performance Quasi-Solid-State Lithium-Sulfur Battery with a Controllably Solidified Cathode−Electrolyte Interface. *ACS Appl. Mater. Interfaces* **2023**, *15*, 19066−19074.
(48) Zhou, T.; Wang, J.; Lv, L.; Li, R.; Chen, L.; Zhang, S.; Zhang, H.; Ma, B.; Huang, J.; Wu, B.; Chen, L.; Deng, T.; Fan, X. Anion-$\pi$ Interaction and Solvent Dehydrogenation Control Enable High-Voltage Lithium-ion Batteries. *Energy Environ. Sci.* **2024**, *17*, 9185−9194.
(49) Tian, K.; Wang, M.; Hu, R.; Li, X.; He, Y.; Song, J.; Zhao, B.; Luo, P.; Li, X.; Cao, G. Continuous $Li^+$ Coordination Polymer Electrolyte for Fast $Li^+$ Migration, Stable Electrolyte Interphases, and Safe Quasi-Solid Lithium Metal Batteries. *ACS Nano* **2025**, *19*, 27768−27781.
(50) Zhao, Y.; Da, X.; Qin, Y.; Jia, X.; Deng, X.; Ding, S.; Xiong, J.; Rong, Q.; Kong, X.; Gao, G. Nonflammable PVDF-based gel polymer electrolytes modified by dimethyl methylphosphate for wide temperature range, long cycle-life and high-safety lithium metal batteries. *Sci. China Mater.* **2024**, *67*, 3994−4004.
(51) Li, P.; Hao, J.; He, S.; Chang, Z.; Li, X.; Wang, R.; Ma, W.; Wang, J.; Lu, Y.; Li, H.; et al. $Li^+$-migration influencing factors and non-destructive life extension of quasi-solid-state polymer electrolytes. *Nat. Commun.* **2025**, *16*, 3727.
(52) Dong, S.; Shi, L.; Zhang, Y.; Geng, S.; Qiang, Z.; Deng, B.; Sun, F.; Huo, H.; Yin, G.; Lou, S. "Pseudo-Charge-Transfer Complex" Electrolyte Enables 490 Wh $kg^{-1}$ Lithium Metal Battery Operated From − 40 to 80 °C. *Angew. Chem., Int. Ed.* **2025**, *64*, No. e202506750.
(53) Huang, X.; Zhao, C.; Kong, W.; Yao, N.; Shuang, Z.; Xu, P.; Sun, S.; Lu, Y.; Huang, W.; Li, J.; Shen, L.; Chen, X.; Huang, J.; Archer, L. A.; Zhang, Q. Tailoring polymer electrolyte solvation for 600 Wh $kg^{-1}$ lithium batteries. *Nature* **2025**, *646*, 343−350.

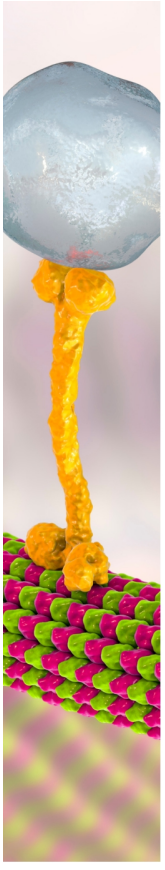




https://doi.org/10.1021/jacs.5c17294
J. Am. Chem. Soc. 2026, 148, 2471−2480